

- 1    **This PDF file includes:**
- 2    Supplementary Notes S1-S2
- 3    Supplementary Tables S1-S10
- 4    Supplementary Figures S1-S21
- 5    Supplementary References
- 6

## S1. Estimation of L/S/IVOC Emissions

The L/S/IVOC emission inventory was developed based on VOC and POA emissions from MEICv1.4, considering the strong correlation between IVOC and VOC emissions and similar definitions of POA and S/LVOCs. In MEICv1.4, emissions are classified into five major source categories (power plants, industry, residential, transportation, and agriculture) and further divided into 22 subcategories. IVOC emissions for each subcategory were estimated using source-specific scaling factors ( $f_{IVOC,i,j}$ ) applied to total VOC emissions, as expressed in Equation S1. S/LVOC emissions resulted from the semi-volatile fraction of POA were estimated using the corresponding scaling factor ( $f_{S/LVOC,i,j}$ ) relative to POA, as shown in Equation S2. IVOC and S/LVOC emissions were then distributed into four volatility bins:  $10^3 \mu\text{g m}^{-3}$  to  $10^6 \mu\text{g m}^{-3}$  for IVOCs and  $10^{-2} \mu\text{g m}^{-3}$  to  $10^2 \mu\text{g m}^{-3}$  for S/LVOCs, with an interval of one order of magnitude per bin. The equations are as follows:

$$E_{IVOC,i,j} = E_{VOC,i,j} * f_{IVOC,i,j} \quad (\text{S1})$$

$$E_{SLVOC,i,j} = E_{POA,i,j} * f_{S/LVOC,i,j} \quad (\text{S2})$$

Here,  $i$  represents the emission source category,  $j$  denotes the volatility bin, and  $E_{IVOC,i,j}$  and  $E_{SLVOC,i,j}$  are the estimated IVOC and S/LVOC emissions (in tons) for each source  $i$  and bin  $j$ . The scaling factors  $f$  were obtained from the literature, with more details provided in Table S3.

## S2. Calculation of glass transition temperature ( $T_g$ ) and viscosity

The glass transition temperature of OA under dry conditions ( $T_{g,org}$ ) is calculated by the Gordon-Taylor equation (Gordon and Taylor, 1952) by assuming the Gordon-Taylor constant ( $k_{GT}$ ) of 1 (Dette et al., 2014):

$$T_{g,org} = \sum_i \omega_i T_{g,i} \quad (\text{S3})$$

where  $\omega_i$  represents the mass fraction of each OA species in CMAQ.

The glass transition temperature of the organic-water mixture ( $T_{g,\omega org}$ ) is determined using the Gordon-Taylor equation, as expressed in Equation (S4):

$$T_{g,\omega_{org}} = \frac{(1-\omega_{org})T_{g,w} + \frac{1}{k_{GT}}\omega_{org}T_{g,org}}{(1-\omega_{org}) + \frac{1}{k_{GT}}\omega_{org}} \quad (S4)$$

where  $k_{GT} = 2.5$  is assumed, and  $T_{g,w}$  (the glass transition temperature of water) is set to 136 K (Kohl et al., 2005). The mass fraction of OA in the particulate phase ( $\omega_{org}$ ) is given by Equation S5:

$$\omega_{org} = \frac{m_{OA}}{m_{OA} + m_{H_2O}} \quad (S5)$$

The mass concentration of water ( $m_{H_2O}$ ) can be determined from the effective hygroscopicity parameter ( $\kappa$ ) of OA:

$$m_{H_2O} = \left( \frac{a_w}{1-a_w} \right) \frac{\kappa \rho_w m_{OA}}{\rho_{OA}} \quad (S6)$$

$$\kappa_{org,i} = 0.11 \frac{OM}{OC} - 0.10 \quad (S7)$$

Here, the  $\kappa_{org}$  of each species was parameterized as a function of OM/OC (Pye et al., 2017).  $\rho_w$  (water density) and  $\rho_{OA}$  (OA density) are assumed to be 1 and 1.44 g cm<sup>-3</sup>, respectively, based on observational experiments in DY. The water activity ( $a_w$ ) is derived from the relative humidity (RH) as  $a_w = RH/100$ .

49 **Supplementary Tables**

50 **Table S1** Statistical metrics of meteorological parameters in DY and GZ.

Parameter	Metrics	DY	GZ	Benchmark
T2 (°C)	OBS	12.99	24.34	
	SIM	13.00	24.32	
	MB	0.01	0.01	$\leq \pm 0.5$
	ME	2.00	1.79	$\leq 2$
	RMSE	2.55	2.39	
RH (%)	OBS	49.14	68.07	
	SIM	46.91	64.20	
	MB	-2.23	-3.87	
	ME	9.79	8.66	
	RMSE	12.87	11.22	
WS (m/s)	OBS	3.82	2.45	
	SIM	5.17	3.19	
	MB	<b>1.34</b>	<b>0.74</b>	$\leq \pm 0.5$
	ME	1.98	1.27	$\leq 2$
	RMSE	2.45	1.59	$\leq 2$
WD (°)	OBS	159.33	94.64	
	SIM	151.39	66.41	
	MB	<b>155.51</b>	<b>63.97</b>	$\leq \pm 10$
	ME	<b>155.52</b>	<b>64.03</b>	$\leq \pm 30$
	RMSE	181.78	107.52	

51 <sup>a</sup> $MB = \frac{1}{N} \sum_{i=1}^N (M_i - O_i)$ ;  $ME = \frac{1}{N} \sum_{i=1}^N |M_i - O_i|$ ;  $RMSE = \left[ \frac{1}{N} \sum_{i=1}^N (M_i - O_i)^2 \right]^{\frac{1}{2}}$ , where  $M_i$   
52 and  $O_i$  represent model predictions and observations, respectively, and  $N$  is the number of data.  
53 The benchmarks refer to Emery and Tai (2001).

54

55

Site	Pollutant	Case	NMB	NME	r
DY	MDA8 O <sub>3</sub>	1D-VBS	-0.09	0.18	0.82
		1D-VBS_E	-0.09	0.18	0.82
		1D-VBS_EY	-0.08	0.18	0.82
		2D-VBS	-0.09	0.18	0.82
	NO <sub>2</sub>	1D-VBS	-0.26	0.49	0.53
		1D-VBS_E	-0.27	0.50	0.53
		1D-VBS_EY	-0.27	0.49	0.53
		2D-VBS	-0.27	0.49	0.53
	SO <sub>2</sub>	1D-VBS	-0.41	0.51	0.47
		1D-VBS_E	-0.41	0.51	0.47
		1D-VBS_EY	-0.41	0.51	0.47
		2D-VBS	-0.41	0.51	0.47
	PM <sub>2.5</sub>	1D-VBS	-0.58	0.58	0.82
		1D-VBS_E	-0.50	0.50	0.84
		1D-VBS_EY	-0.46	0.46	0.84
		2D-VBS	-0.46	0.46	0.83
GZ	MDA8 O <sub>3</sub>	1D-VBS	0.26	0.49	0.38
		1D-VBS_E	0.25	0.49	0.38
		1D-VBS_EY	0.25	0.48	0.38
		2D-VBS	0.26	0.49	0.38
	NO <sub>2</sub>	1D-VBS	-0.42	0.53	0.33
		1D-VBS_E	-0.42	0.53	0.33
		1D-VBS_EY	-0.42	0.53	0.33
		2D-VBS	-0.42	0.53	0.33
	SO <sub>2</sub>	1D-VBS	-0.46	0.78	0.48
		1D-VBS_E	-0.46	0.78	0.48
		1D-VBS_EY	-0.46	0.78	0.48

		2D-VBS	-0.46	0.78	0.48
		1D-VBS	-0.48	0.50	0.33
		1D-VBS_E	-0.35	0.40	0.37
	PM <sub>2.5</sub>	1D-VBS_EY	-0.19	0.32	0.37
		2D-VBS	-0.31	0.38	0.45

57 <sup>a</sup>Benchmark values are NMB<±0.15, NME<0.25, and R>0.5 for MDA8 O<sub>3</sub>, NMB<±0.3,  
 58 NME<0.5, and R>0.4 for 24-hr average PM<sub>2.5</sub>,  $NMB = \frac{\sum_{i=1}^N (M_i - O_i)}{\sum_{i=1}^N O_i}$ ;  $NME = \frac{\sum_{i=1}^N |M_i - O_i|}{\sum_{i=1}^N O_i}$ ;  $r =$   
 59  $\frac{\sum_{i=1}^N [(M_i - \bar{M}) \times (O_i - \bar{O})]}{\sqrt{\sum_{i=1}^N (M_i - \bar{M})^2 \times \sum_{i=1}^N (O_i - \bar{O})^2}}$ , where M<sub>i</sub> and O<sub>i</sub> represent model predictions and observations,  $\bar{M}$   
 60 and  $\bar{O}$  represent the mean of predictions and observations, and N is the number of data (Emery  
 61 et al., 2017).  
 62

63 **Table S3** Source-specific scaling factors for emissions of L/SVOCs ( $\log_{10}C^*(\mu\text{g m}^{-3})\leq 2$ ) derived from POA emissions, and IVOCs ( $3\leq\log_{10}C^*(\mu\text{g m}^{-3})\leq 6$ )  
64 derived from VOC emissions in this study.

Sector	Subsector	Fractions for logC*(μg m <sup>-3</sup> , at 298K) bins									Ref.
		<i>f<sub>L/SVOC,i,j</sub></i>					<i>f<sub>IVOC,i,j</sub></i>				
		≤-2	-1	0	1	2	3	4	5	6	
Power	Power plants	0.2443	0.1304	0.0727	0.1454	0.4071	0.1880	0.1500	0.2260	0.1130	Chang et al. (2022)
Industry	industrial boiler	0.2443	0.1304	0.0727	0.1454	0.4071	0.1880	0.1500	0.2260	0.1130	
	heat supply										
	Cement										
	Coking	0.2355	0.1742	0.0805	0.0806	0.4291	0.0082	0.0075	0.0025	0.0017	
	Iron and steel										
	Petrochemicals										
	Oil and gas storage	0.0000	0.0000	0.0000	0.0000	0.0000	0.0000	0.0000	0.0000	0.12	a
	Industrial Painting					0.0025 <sup>c</sup>	0.0127	0.0329	0.0405	0.1645	Mcdonald
	architectural coating	0.0000	0.0000	0.0000	0.0000	0.0022 <sup>c</sup>	0.0119	0.0290	0.0358	0.1455	et al.
	printing					0.0021 <sup>c</sup>	0.0103	0.0269	0.0331	0.1346	(2018)
	Other industrial sectors	0.5430	0.0958	0.0468	0.0614	0.2531	0.0385	0.0410	0.0563	0.1132	b

Residential	Domestic combustion	0.1072	0.2914	0.0377	0.0708	0.4928	0.0390	0.3170	0.2540	0.1200	Chang et al. (2022)   <sup>b</sup>
	Domestic biomass combustion	0.4395	0.1923	0.0680	0.1387	0.1615	0.0690	0.1710	0.0480	0.0700	
	Domestic VCP	0.0000	0.0000	0.0000	0.0000	0.0030 <sup>c</sup>	0.0156	0.0383	0.0469	0.1926	
	Other domestic sources	0.5156	0.1612	0.0352	0.0698	0.2181	0.0412	0.1754	0.1163	0.1275	
Transportation	Gasoline Vehicles	0.9869	0.0000	0.0031	0.0051	0.0045	0.0061	0.0206	0.0568	0.0943	Tang et al. (2021)   <sup>d</sup>  Tang et al. (2021)   <sup>f</sup>
	Diesel Vehicles	0.1321	0.0546	0.0858	0.3641	0.3633	0.0540	0.1490	0.1870	0.1590	
	Motorcycles	0.9869	0.0000	0.0031	0.0051	0.0045	0.0061	0.0206	0.0568	0.0943	
	Non-Road transportation	0.7801	0.0307	0.0399	0.0645	0.0849	0.0147	0.0344	0.0684	0.0787	
Agriculture	Fertilizer Application	0.0000	0.0000	0.0000	0.0000	0.0000	0.0000	0.0000	0.0000	0.0000	Chang et al. (2022)
	Livestock Farming										

65 <sup>a</sup> Data from the California Air Resources Board's 2015 Consumer and Commercial Products Survey (CARB, 2019);

66 <sup>b</sup> Average values of subsectors under the same sector;

67 <sup>c</sup> Since volatile chemical product emissions are closely correlated with VOC emissions, the SVOC emissions for this sector were estimated based on VOC  
68 emissions.



69 <sup>d</sup> The IVOC scaling factors for diesel vehicles were referenced from Lu et al. (2020) , while the SVOC scaling factors were based on the work of An et al.  
70 (2023).

71 <sup>f</sup> For non-road mobile sources, scaling factors for agricultural machinery (Che et al., 2023) , road construction machinery (Shen et al., 2023), and ships (An et  
72 al., 2023), were used. The contributions of different sources to non-road mobile sources were obtained from Huang et al. (2018) and Zhao et al. (2022).

73 **Table S4** Annual emissions of IVOCs and SVOCs (Unit: Tg) from different emission sources  
74 in China in 2018.

Sector	IVOCs	SVOCs
Industry and Power	1.17	0.34
Residential	1.91	2.69
Transportation	0.90	0.15
Solvent use	2.69	/
Total	6.68	3.18

75

76 **Table S5** Mole-based SOA yields for aromatics and PAHs used in this study.

Case	Precur- sor	High NOx						Ref
		10E-06	0.01	0.1	1	10	100	
1D-VBS	Benzene	0.0000	0.0000	0.0000	0.0340	0.0000	0.3920	Qin et al. (2021)
	Toluene	0.0000	0.0000	0.0000	0.0160	0.0510	0.0470	
	Xylene	0.0000	0.0000	0.0000	0.0150	0.0230	0.0600	
	PAHs	0.0000	0.0000	0.0000	0.0280	0.0225	0.0280	
	Precur- sor	Low NOx						Ref
	10E-06	0.01	0.1	1	10	100		
	Benzene	0.0000	0.1460	0.0000	0.0000	0.0000	0.0000	Qin et al. (2021)
	Toluene	0.0000	0.1400	0.0000	0.0000	0.0000	0.0000	
	Xylene	0.0000	0.1930	0.0000	0.0000	0.0000	0.0000	
	PAHs	0.0000	0.0473	0.0000	0.0000	0.0000	0.0000	
Case	Precur- sor	High NOx						Ref
		10E-06	0.01	0.1	1	10	100	
1D-VBS_EY	Benzene	0.0000	0.0000	0.1874	0.1559	0.0000	0.0000	Bilsback et al. (2023)
	Toluene	0.0000	0.0000	0.1358	0.0967	0.0000	0.0000	
	Xylene	0.0000	0.0000	0.0284	0.0049	0.0040	0.1581	
	PAHs <sup>a</sup>	0.0000	0.1183	0.0988	0.1269	0.2110	0.0000	
	Precur- sor	Low NOx						Ref
	10E-06	0.01	0.1	1	10	100		
	Benzene	0.0017	0.0131	0.0000	0.0592	0.1732	0.0000	Bilsback et al. (2023)
	Toluene	0.0007	0.0299	0.0000	0.0703	0.1584	0.0000	
	Xylene	0.0106	0.0000	0.1452	0.0000	0.0422	1.3439	
	PAHs <sup>a</sup>	0.0230	0.0600	0.0381	0.0572	0.1753	0.0000	

77 <sup>a</sup> The parameters for PAHs adopted naphthalene SOA yields from Bilsback et al. (2023).

79 **Table S6** Summary of O/C ratios for POA factors in eastern China reported in prior measure-  
80 ments.

Site	HOA	BBOA	CCOA	COA	NOA	Ref
Dongying	0.55	0.37	/	/	/	Feng et al. (2023)
Guangzhou	0.2	/	/	0.19	0.5	Chen et al. (2021)
Gucheng	0.13	0.44	0.15	/	/	Zhang et al. (2022)
Beijing	0.16	0.29	0.19	0.16	/	Xu et al. (2021)
Nanjing	0.12	/	/	0.27	/	Xian et al. (2023)
Nanjing	0.17	0.49	/	/	/	Gu et al. (2022)
Shanghai	0.15	/	/	0.29	/	Zhu et al. (2021)
Hangzhou	0.07	/	/	0.18/	/	Li et al. (2018)
Yangzhou	0.25	0.45	/	0.36	/	(Ge et al., 2017)
Average	0.2	0.41	0.17	0.24	0.5	

82 **Table S7** OA surrogate species in the 1D-VBS and their physicochemical properties at 298K,  
83 including saturated vapor pressure ( $C_0^*$ ), organic matter to organic carbon ratio (OM/OC), mo-  
84 lecular weight ( $\tilde{M}$ ), and oxygen to carbon ratio (O/C).

Species	Description	$C_0^*$	OM/OC	$\tilde{M}$	O/C	Ref
AAVB1	ASOA	0.01	2.7	198.0	1.227	Qin et al. (2021)
AAVB2		1	2.35	179.0	0.947	
AAVB3		10	2.17	169.0	0.803	
AAVB4		100	1.99	158.0	0.659	
AAVB5 <sup>a</sup>		0.1	2.53	189.0	1.091	Newly added
AAVB6 <sup>a</sup>		1E-06	3.41	229.0	1.797	
AOLGA	Oligomers derived from ASOA	1E-10	2.50	206.0	1.067	Pye et al. (2017)
AIETET	2-methyltetrols (2-MT)	1E-10	2.27	136.15	0.833	Pye et al. (2013)
AIEOS	IEPOX-derived organic sulfates	1E-10	3.60	216.2	1.947	
AIMGA	2-methylglyceric acid (2-MG)	1E-10	2.50	120.1	1.067	
AIMOS	MPAN-derived organic nitrates	1E-10	4.17	200.16	2.403	
ADIM	Dimers	1E-10	2.07	248.23	0.723	Pye et al. (2015)
AISO1	Semi-volatile iso-	116.01	2.20	132.0	0.827	
AISO2	prene SOA	0.617	2.23	133.0	0.857	
AISOPNN	Semi-volatile SOA from iso-prene dinitrates produced from NO <sub>3</sub> reaction	8.9	3.80	226.0	2.107	
AMT1	Monoterpene SOA from OH/O <sub>3</sub> -initiated oxidation	0.01	1.67	300.0	0.4	Xu et al. (2018)
AMT2		0.1	1.67	200.0	0.4	
AMT3		1	1.72	186.0	0.444	
AMT4		10	1.53	184.0	0.3	
AMT5		100	1.57	170.0	0.333	
AMT6		1000	1.40	168.0	0.2	
AMTNO3	Semi-volatile SOA from	12.0	1.90	231.0	0.587	Pye et al. (2015)

	monoterpene ni- trates (excluding $\alpha$ -pinene) Nonvolatile or- ganic hydrolysis					
AMTHYD	product of MTNO <sub>3</sub> <sup>b</sup> and ISOPNN <sup>c</sup>	1E-10	1.54	186.0	0.299	
ASQT	Sesquiterpene SOA	24.984	1.52	273.0	0.283	Carlton et al. (2010); Pye et al. (2017)
AOLGB	oligomers derived from BSOA	1E-10	2.10	248.0	0.747	Carlton et al. (2010); Pye et al. (2017)
AGLY	OA from glyoxal and methylglyoxal uptake onto accu- mulation-mode particles OA from aqueous- phase oxidation of	1E-10	2.13	66.4	0.771	Pye et al. (2015)
AORGC	glyoxal and methylglyoxal in cloud droplets	1E-10	2.00	177.0	0.677	Carlton et al. (2008)
APNCOM	Non-carbon frac- tion of POA	1E-10	1.60	220.0	0.347	Simon and Bhawe (2012)
APOC	Carbon fraction of POA					
ALVPO1		0.1	1.39	218.0	0.185	Murphy et al. (2017)
ASVPO1		1	1.32	230.0	0.123	
ASVPO2		10	1.26	241.0	0.073	
ASVPO3		100	1.21	253.0	0.032	
AIVPO1	Semi-volatile	1000	1.17	266.0	0.00	
ALVOO1	POA	0.01	2.27	136.0	0.886	
ALVOO2		0.1	2.06	136.0	0.711	
ASVOO1		1	1.88	135.0	0.567	
ASVOO2		10	1.73	135.0	0.477	
ASVOO3		100	1.60	134.0	0.345	

- 86    <sup>b</sup> MTNO<sub>3</sub>: Monoterpene-derived organic nitrates.
- 87    <sup>c</sup> ISOPNN: Second generation isoprene dinitrate from NO<sub>3</sub> reaction
- 88    .

**Table S8** OA surrogate species in the 2D-VBS and their physicochemical properties at 298 K (Zhao et al., 2015; Chang et al., 2022), including saturated vapor pressure ( $C_o^*$ ), organic matter to organic carbon ratio (OM/OC), molecular weight ( $\tilde{M}$ ), and oxygen to carbon ratio (O/C).

Species	$C_o^*$	OM/OC	$\tilde{M}$	O/C
AM120	0.01	3.667	152.30	2.0
A0020	1	3.667	141.00	2.0
A0120	10	3.667	129.70	2.0
A0220	100	3.667	118.50	2.0
A0320	1000	3.667	107.20	2.0
A0420	1.0E+04	3.667	95.90	2.0
A0520	1.0E+05	3.667	84.60	2.0
A0620	1.0E+06	3.667	73.30	2.0
A0720	1.0E+07	3.667	62.10	2.0
AM115	0.01	3.041	161.60	1.5
A0015	1	3.041	149.60	1.5
A0115	10	3.041	137.60	1.5
A0215	100	3.041	125.70	1.5
A0315	1000	3.041	113.70	1.5
A0415	1.0E+04	3.041	101.70	1.5
A0515	1.0E+05	3.041	89.80	1.5
A0615	1.0E+06	3.041	77.80	1.5
A0715	1.0E+07	3.041	65.80	1.5
AM110	0.01	2.417	178.00	1.0
A0010	1	2.417	164.80	1.0
A0110	10	2.417	151.60	1.0
A0210	100	2.417	138.40	1.0
A0310	1000	2.417	125.20	1.0
A0410	1.0E+04	2.417	112.00	1.0
A0510	1.0E+05	2.417	98.90	1.0
A0610	1.0E+06	2.417	85.70	1.0
A0710	1.0E+07	2.417	72.50	1.0
AM107	0.01	2.042	195.70	0.7
A0007	1	2.042	181.20	0.7
A0107	10	2.042	166.70	0.7
A0207	100	2.042	152.20	0.7
A0307	1000	2.042	137.70	0.7



A0407	1.0E+04	2.042	123.20	0.7
A0507	1.0E+05	2.042	108.70	0.7
A0607	1.0E+06	2.042	94.20	0.7
A0707	1.0E+07	2.042	79.70	0.7
AM104	0.01	1.667	228.80	0.4
A0004	1	1.667	211.90	0.4
A0104	10	1.667	194.90	0.4
A0204	100	1.667	178.00	0.4
A0304	1000	1.667	161.00	0.4
A0404	1.0E+04	1.667	144.10	0.4
A0504	1.0E+05	1.667	127.10	0.4
A0604	1.0E+06	1.667	110.20	0.4
A0704	1.0E+07	1.667	93.20	0.4
AM102	0.01	1.417	273.20	0.2
A0002	1	1.417	253.00	0.2
A0102	10	1.417	232.70	0.2
A0202	100	1.417	212.50	0.2
A0302	1000	1.417	192.30	0.2
A0402	1.0E+04	1.417	172.00	0.2
A0502	1.0E+05	1.417	151.80	0.2
A0602	1.0E+06	1.417	131.50	0.2
A0702	1.0E+07	1.417	111.30	0.2
AM101	0.01	1.292	312.30	0.1
A0001	1	1.292	289.20	0.1
A0101	10	1.292	266.00	0.1
A0201	100	1.292	242.90	0.1
A0301	1000	1.292	219.80	0.1
A0401	1.0E+04	1.292	196.60	0.1
A0501	1.0E+05	1.292	173.50	0.1
A0601	1.0E+06	1.292	150.40	0.1
A0701	1.0E+07	1.292	127.20	0.1
AM100	0.01	1.167	378.00	0.0
A0000	1	1.167	350.00	0.0
A0100	10	1.167	322.00	0.0
A0200	100	1.167	294.00	0.0
A0300	1000	1.167	266.00	0.0
A0400	1.0E+04	1.167	238.00	0.0

A0500	1.0E+05	1.167	210.00	0.0
A0600	1.0E+06	1.167	182.00	0.0
A0700	1.0E+07	1.167	154.00	0.0
ADIM	1E-10	2.07	248.23	0.723
AGLY	1E-10	2.13	66.4	0.771
AIEOS	1E-10	3.60	216.2	1.947
AIETET	1E-10	2.27	136.15	0.833
AIMGA	1E-10	2.50	120.1	1.067
AIMOS	1E-10	4.17	200.16	2.403
AISO1	116.01	2.20	132.0	0.827
AISO2	0.617	2.23	133.0	0.857
AISO3	1E-10	2.80	168.2	1.307
AISOPNN	8.9	3.80	226.0	2.107
AMTNO3	12.0	1.90	231.0	0.587
AMTHYD	1E-10	1.54	186.0	0.299
AOLGB	1E-10	2.10	248.0	0.747

---

92 Note: While ASOA, BSOA, and POA are separately represented in the model, species with  
93 identical volatility and O/C are assumed to share physicochemical properties and are not listed  
94 individually in this table.

95 **Table S9** Contribution of SOA to OA in different simulations.

Site	Case	SIM	OBS
DY	1D-VBS	59%	72%
	1D-VBS_E	62%	
	1D-VBS_EY	67%	
	2D-VBS	82%	
GZ	1D-VBS	78%	64%
	1D-VBS_E	72%	
	1D-VBS_EY	77%	
	2D-VBS	84%	

97 **Table S10** CMAQ performance in hourly OA, SOA and POA simulations.

Site	Pollu- tant	Case	NMB	NME	r
DY	OA	1D-VBS	-0.67	0.67	0.87
		1D-VBS_E	-0.37	0.39	0.85
		1D-VBS_EY	-0.27	0.36	0.84
		2D-VBS	-0.24	0.38	0.83
	SOA	1D-VBS	-0.72	0.72	0.78
		1D-VBS_E	-0.45	0.49	0.74
		1D-VBS_EY	-0.30	0.43	0.75
		2D-VBS	-0.11	0.41	0.75
	POA	1D-VBS	-0.55	0.55	0.80
		1D-VBS_E	-0.20	0.30	0.84
		1D-VBS_EY	-0.21	0.30	0.84
		2D-VBS	-0.54	0.54	0.86
GZ	OA	1D-VBS	-0.72	0.72	0.34
		1D-VBS_E	-0.44	0.48	0.33
		1D-VBS_EY	-0.34	0.41	0.33
		2D-VBS	-0.24	0.36	0.39
	SOA	1D-VBS	-0.71	0.71	0.46
		1D-VBS_E	-0.47	0.48	0.44
		1D-VBS_EY	-0.33	0.39	0.43
		2D-VBS	-0.14	0.33	0.43
	POA	1D-VBS	-0.76	0.76	0.05
		1D-VBS_E	-0.40	0.60	0.06
		1D-VBS_EY	-0.41	0.61	0.07
		2D-VBS	-0.53	0.60	0.35

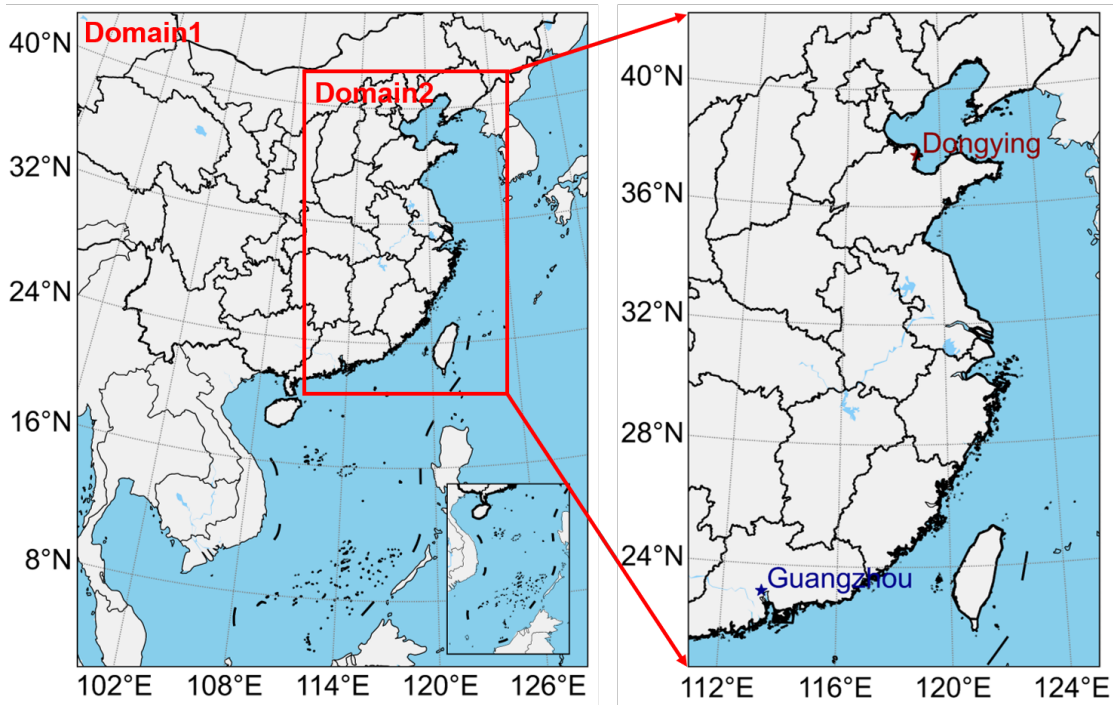


**Figure S1** Modeling domains and locations of observational sites Dongying (DY) and Guangzhou (GZ).



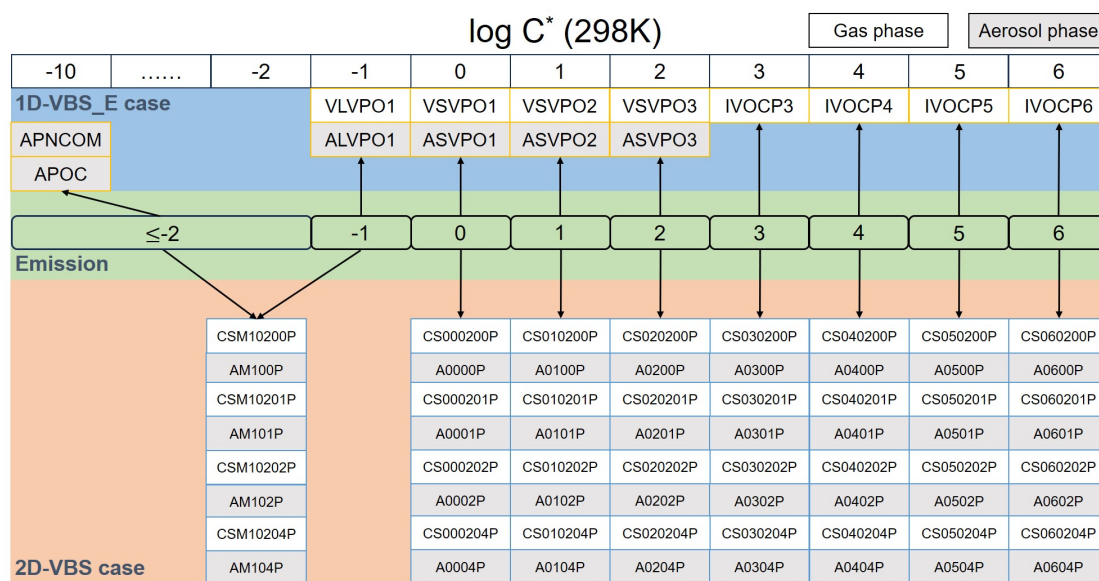
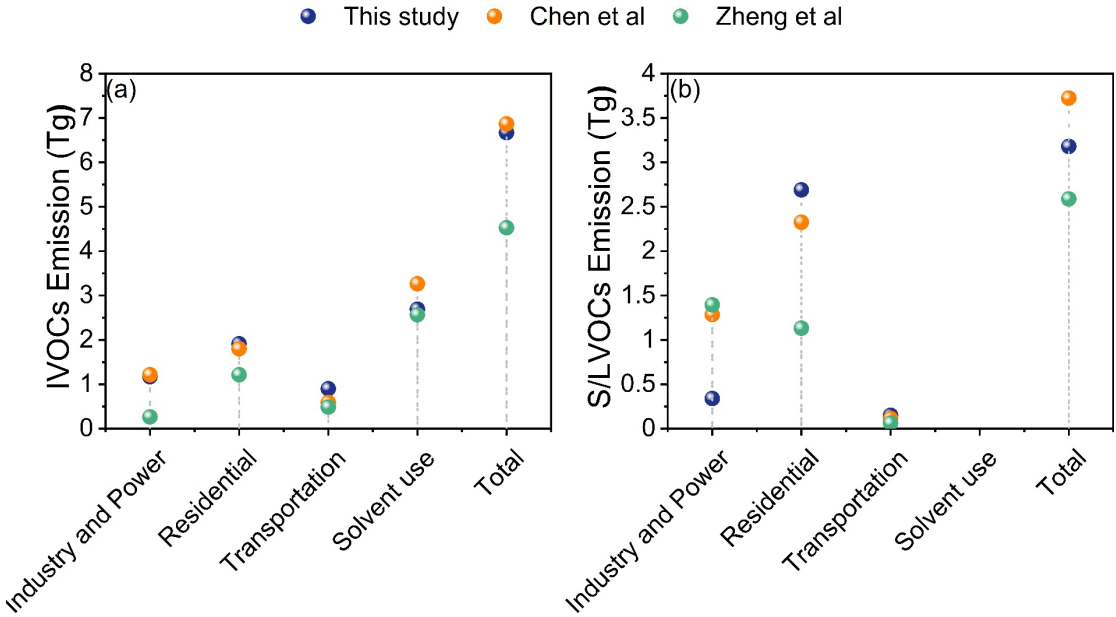


**Figure S3** Volatility distribution of L/S/IVOC emissions in the 1D-VBS\_Y and 2D-VBS simulations. The green area shows L/S/IVOC emission estimates. The blue and orange areas represent allocation of these emissions across volatility bins in the 1D-VBS\_E and 2D-VBS simulations, respectively. Grey boxes denote aerosol phase, and white boxes indicate gas phase.



119

120 **Figure S4** Comparison of annual emissions of (a) IVOC and (b) S/LVOC emissions in China

121 in 2018 from this study with the estimates from Chen et al. (2024) and Zheng et al. (2023).

122



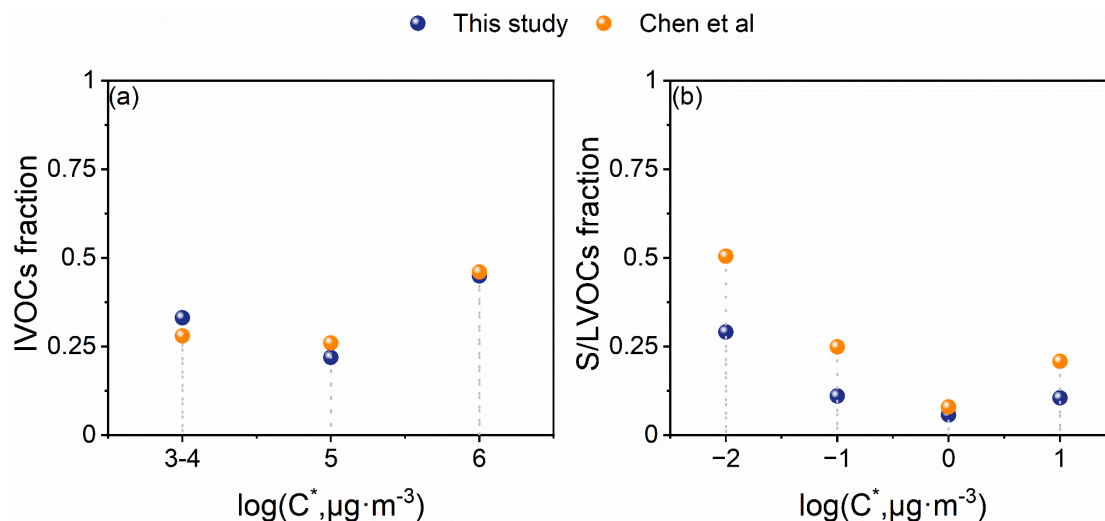


**Figure S5** Comparison of the volatility distributions of (a) IVOC and (b) S/LVOC emissions across all volatility bins in China in 2018 between this study and estimates from Chen et al. (2024).

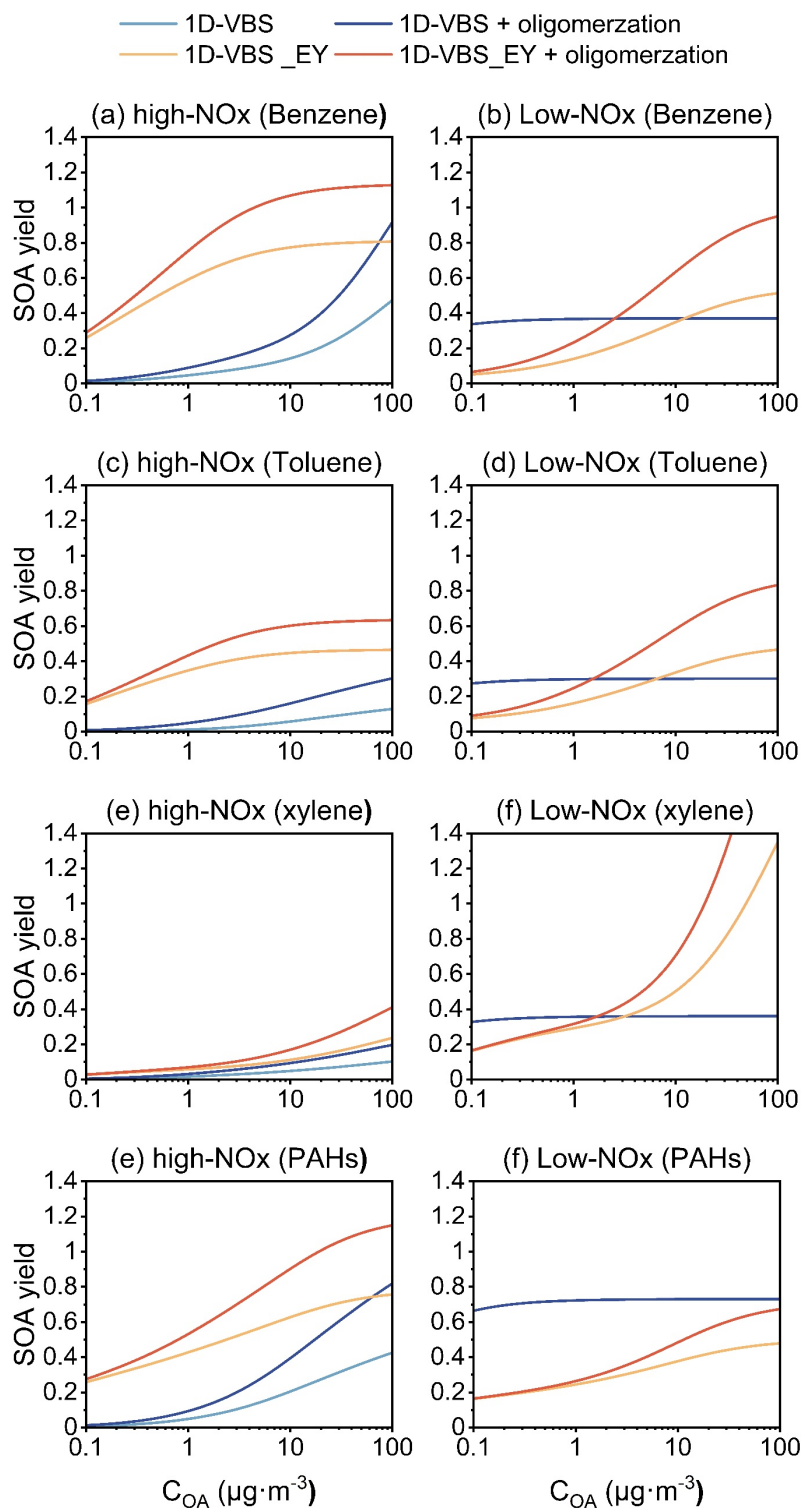


**Figure S6** SOA mass yield from aromatic hydrocarbons (a, b: benzene; c, d: toluene; e, f: xylene; g, h: PAHs) under high-NOx and low-NOx conditions.

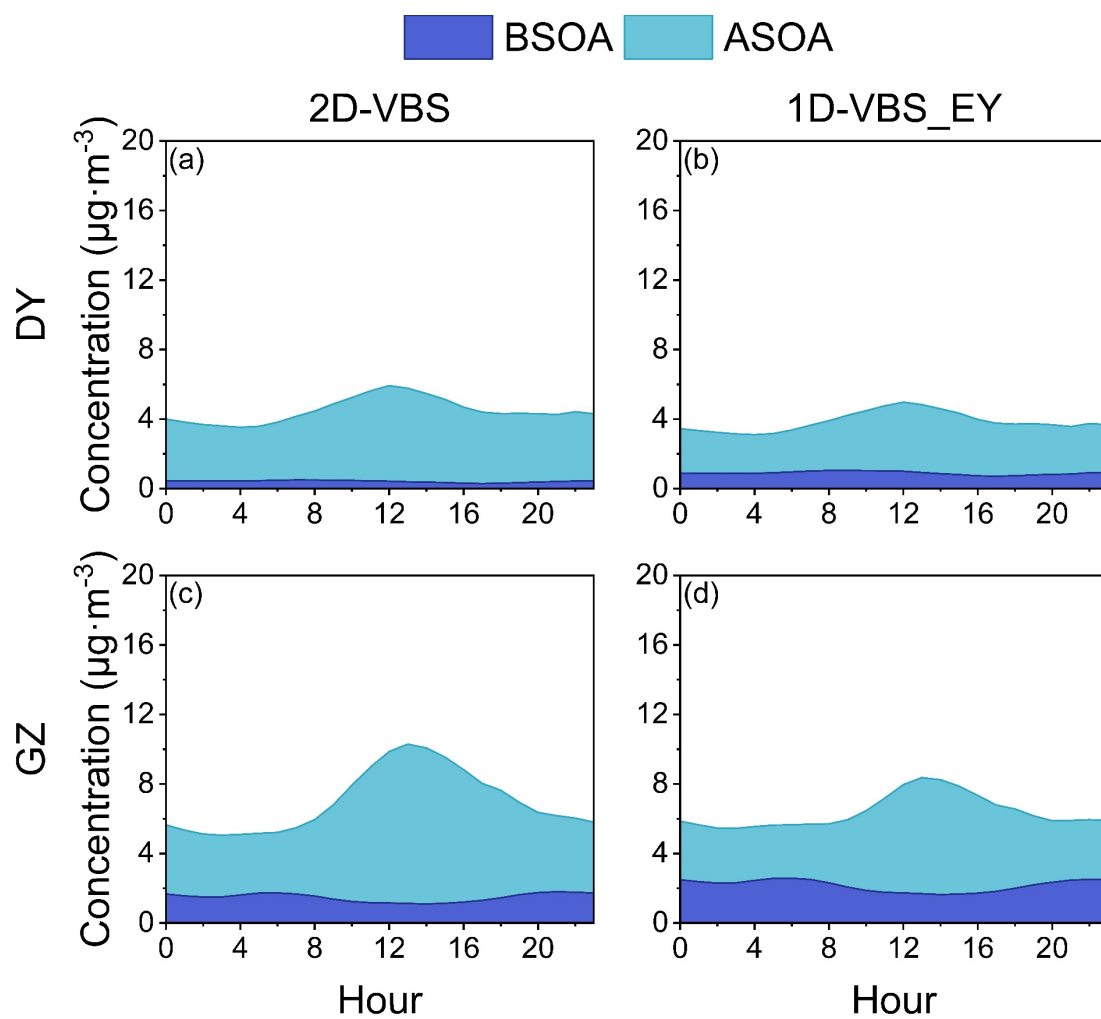


**Figure S7** Diurnal variations of SOA compositions (ASOA and BSOA) from 1D-VBS\_EY and 2D-VBS simulations in DY (a-b) and GZ (c-d).

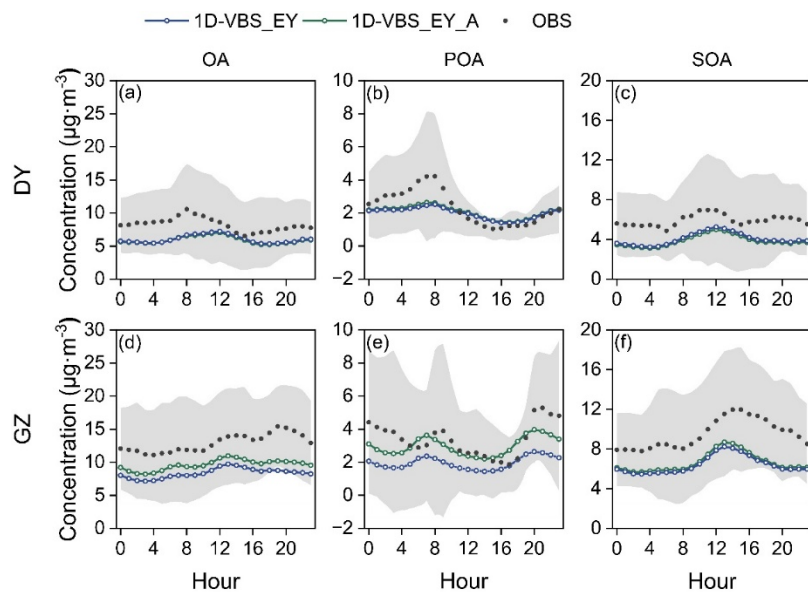


**Figure S8** Simulated diurnal variations of OA, POA, and SOA at DY (a–c) and GZ (d–f) compared with observations. Blue lines represent the 1D-VBS\_EY case, and green lines represent the sensitivity case (1D-VBS\_EY\_A) with scaled POA emissions. Black dots denote observations. The light grey shading indicates the standard deviations ( $\pm 1\sigma$ ) from the mean concentrations in the observations.

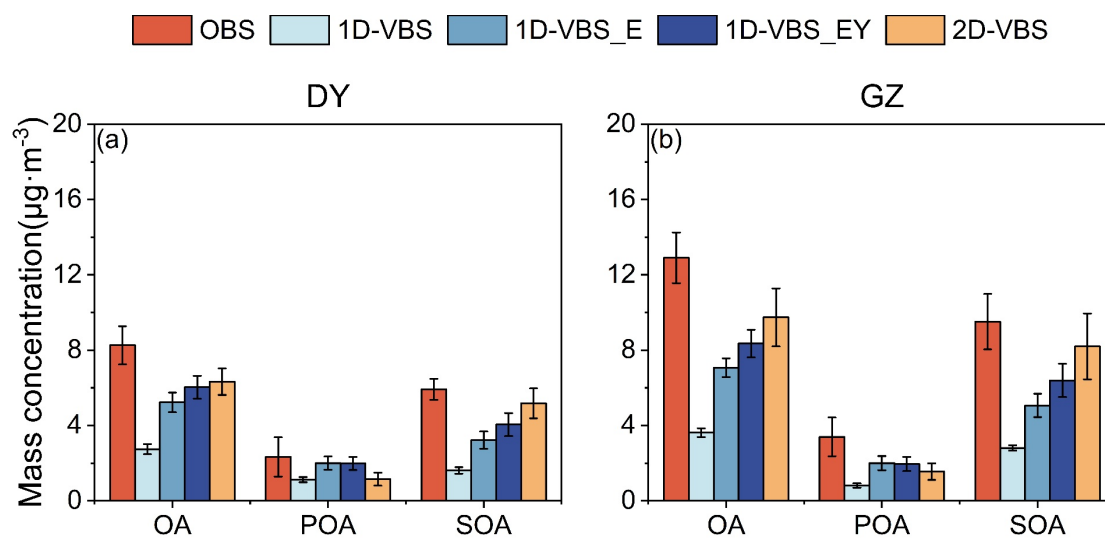


**Figure S9** Period-averaged mass concentrations of modeled and observed OA, POA, and SOA in DY (a) and GZ (b), with BBOA and COA excluded from the OA and POA observations.

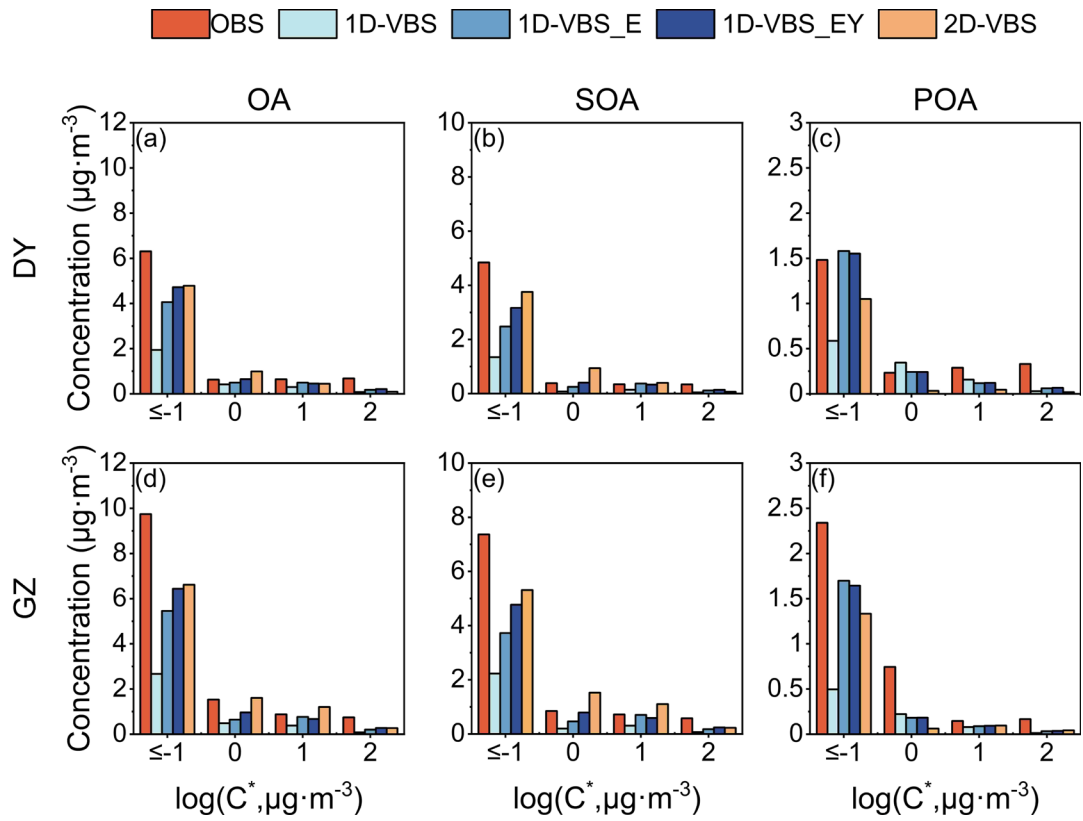


**Figure S10** Simulated mass concentrations of OA, POA, and SOA across volatility bins with  $C^*$  ranging from  $<10^{-1}$  to  $10^2 \mu\text{g m}^{-3}$ , compared to observations in DY (a-c) and GZ (d-f).

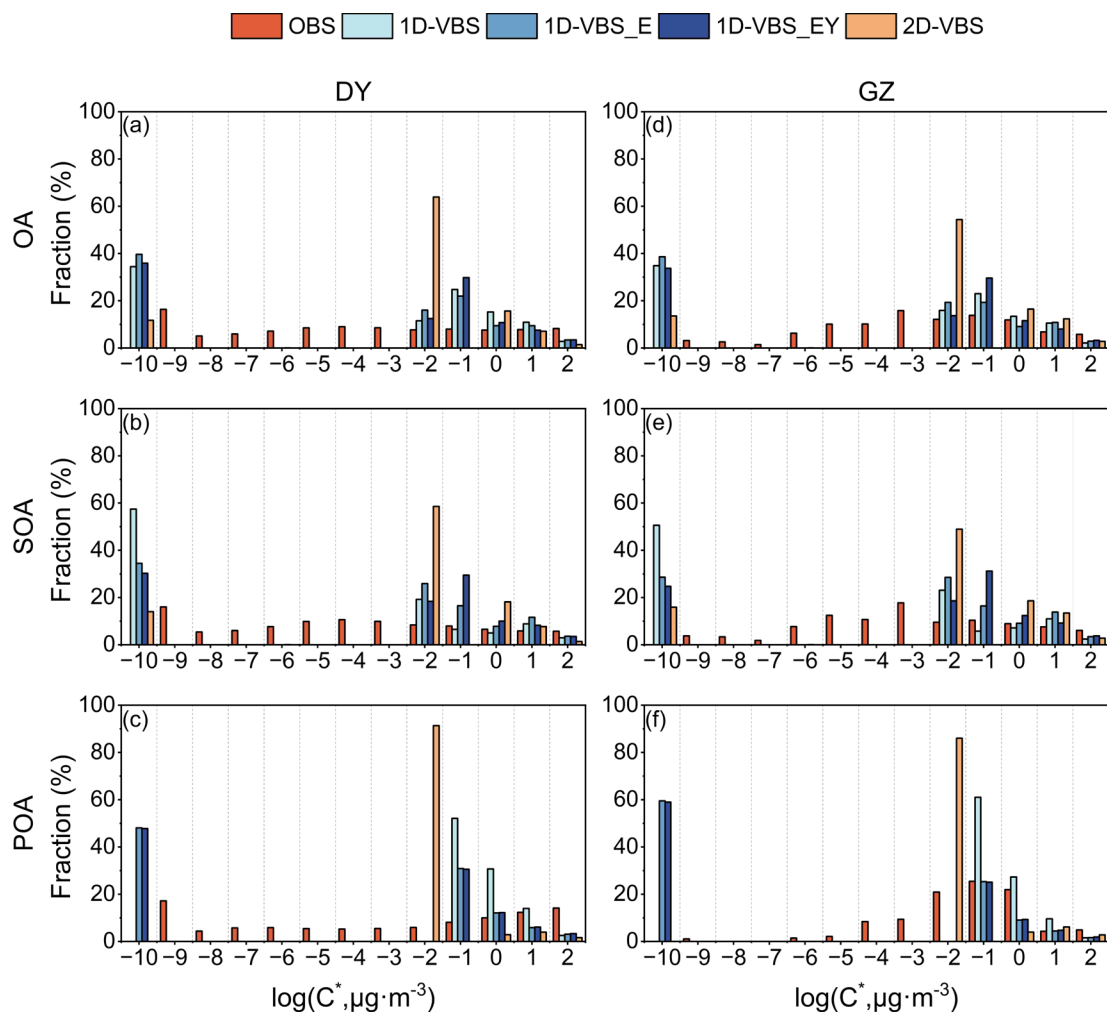


**Figure S11** Simulated OA, POA, and SOA volatility distributions across volatility bins with  $C^*$  ranging from  $10^{-10}$  to  $10^2 \mu\text{g m}^{-3}$ , compared to the observations in DY (a-c) and GZ (d-f).

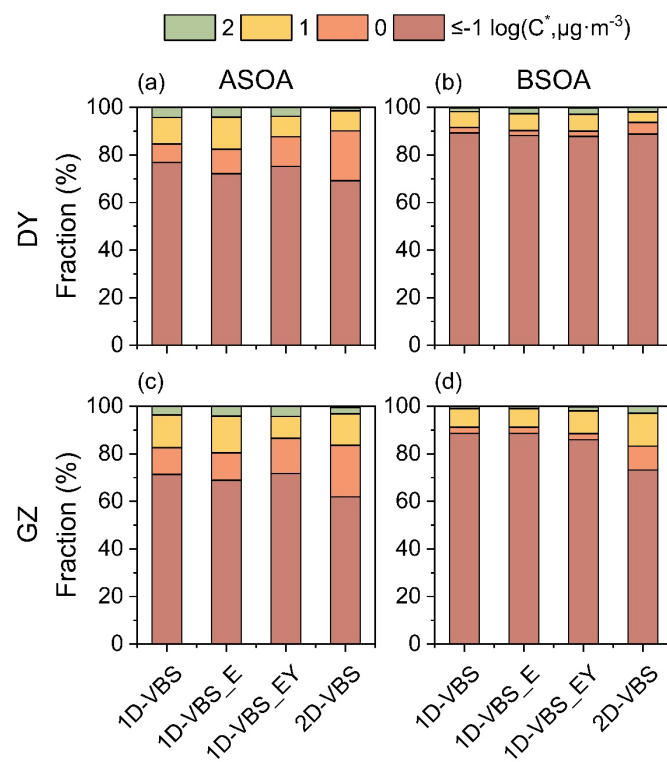


**Figure S12** Simulated volatility distributions of BSOA and ASOA in DY (a-b) and GZ (c-d).



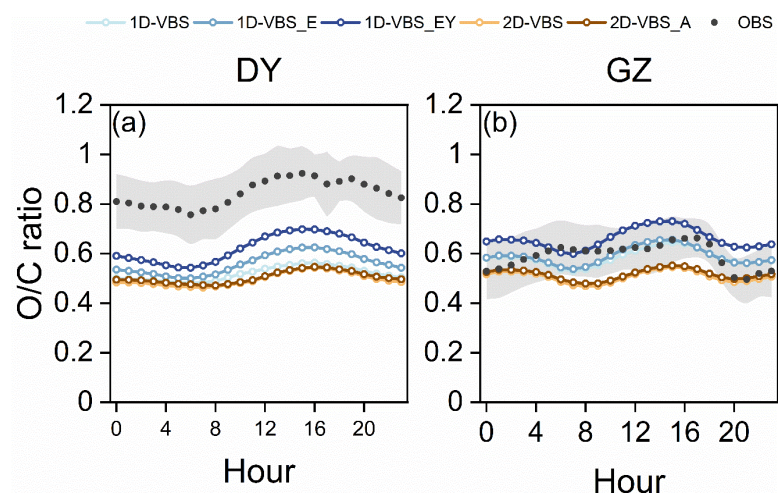


**Figure S13** Simulated diurnal variations of OA O/C ratios compared to observations in DY (a) and GZ (b).

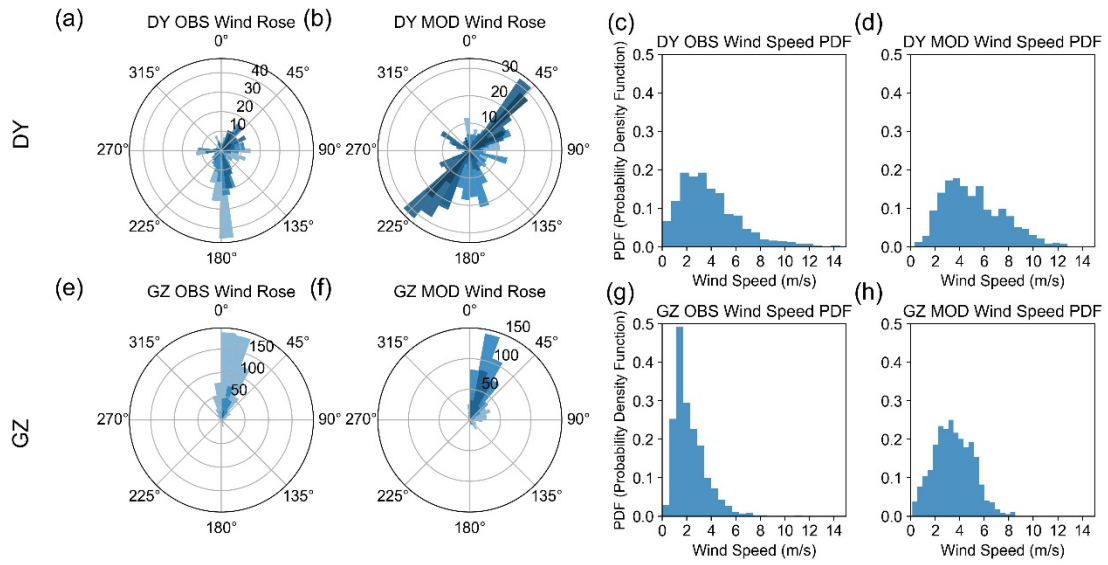


**Figure S14** Observed and simulated wind roses and wind speed probability density functions (PDFs) at the DY (a–d) and GZ (e–h) sites.

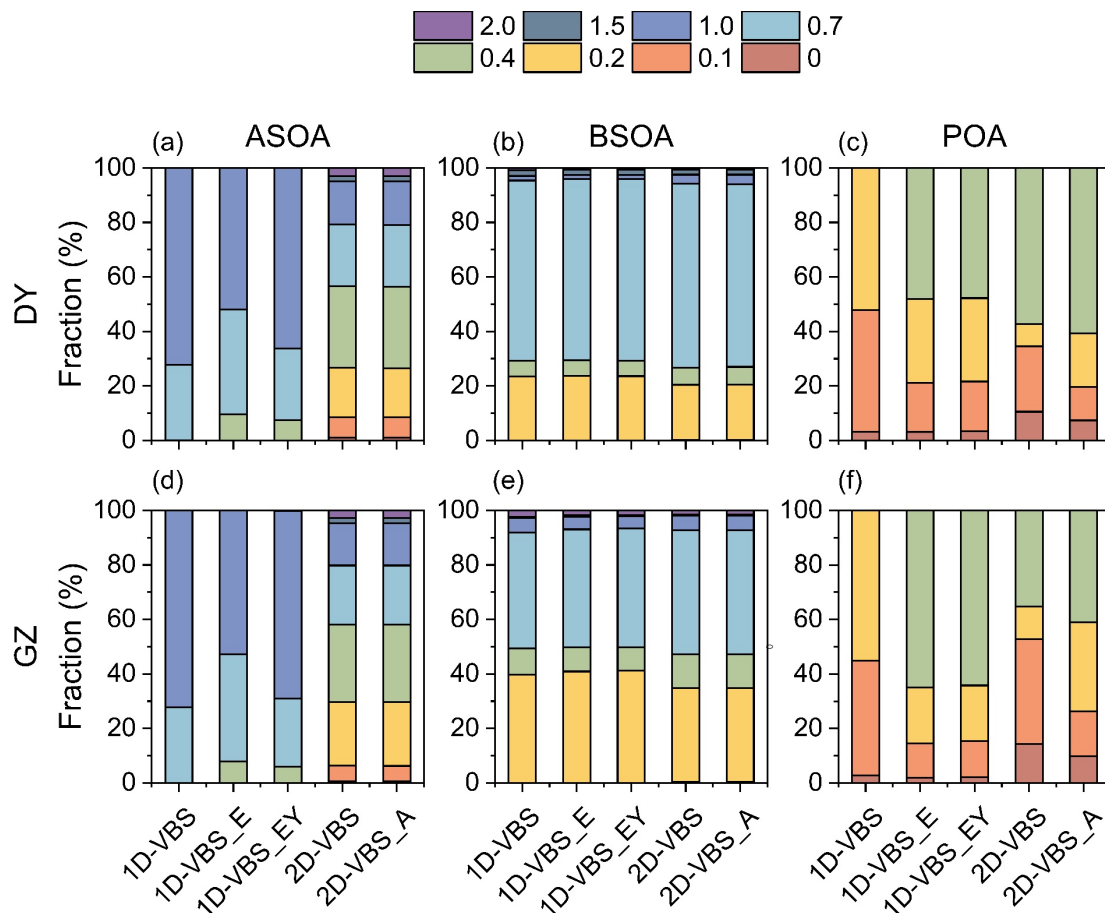


**Figure S15** Mass contributions of ASOA, BSOA and POA across O/C bins in DY (a-c) and GZ(d-f). The numbers in the legends represent median O/C values.

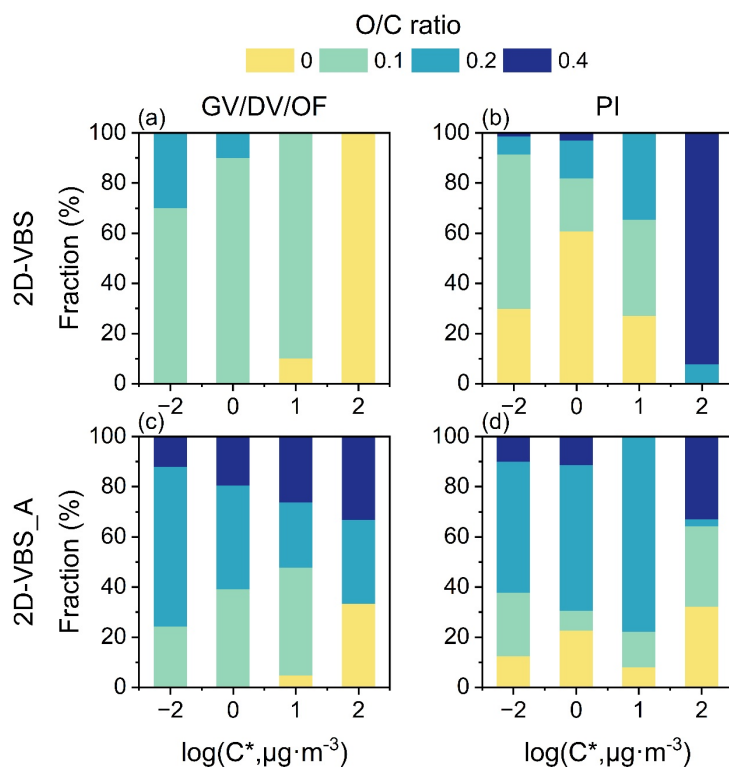


**Figure S16** O/C distributions of L/SVOC emissions from gasoline/diesel vehicles or off-road mobile sources (GV/DV/OF), and power plants or industrial sources (PI) in the 2D-VBS simulation (a–b) and the 2D-VBS\_A simulation (c–d).

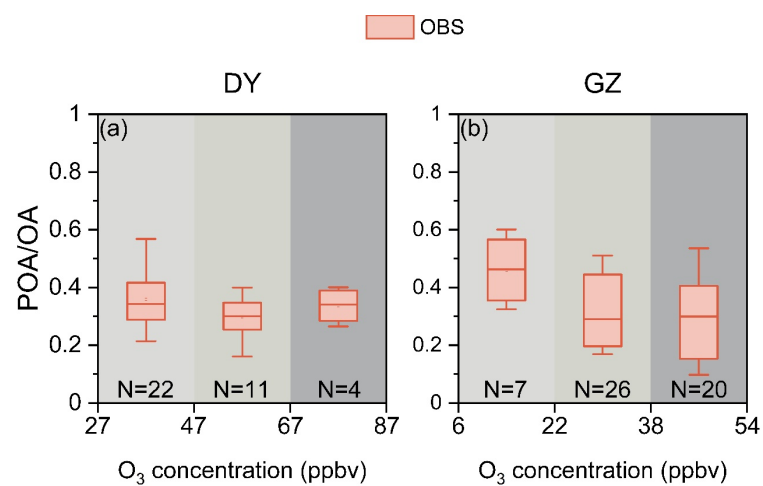


**Figure S17** Variation of POA/OA ratios with daily average ozone concentrations in the observations in DY (a) and GZ (b). N denotes the sample size of POA/OA ratios within each ozone interval.

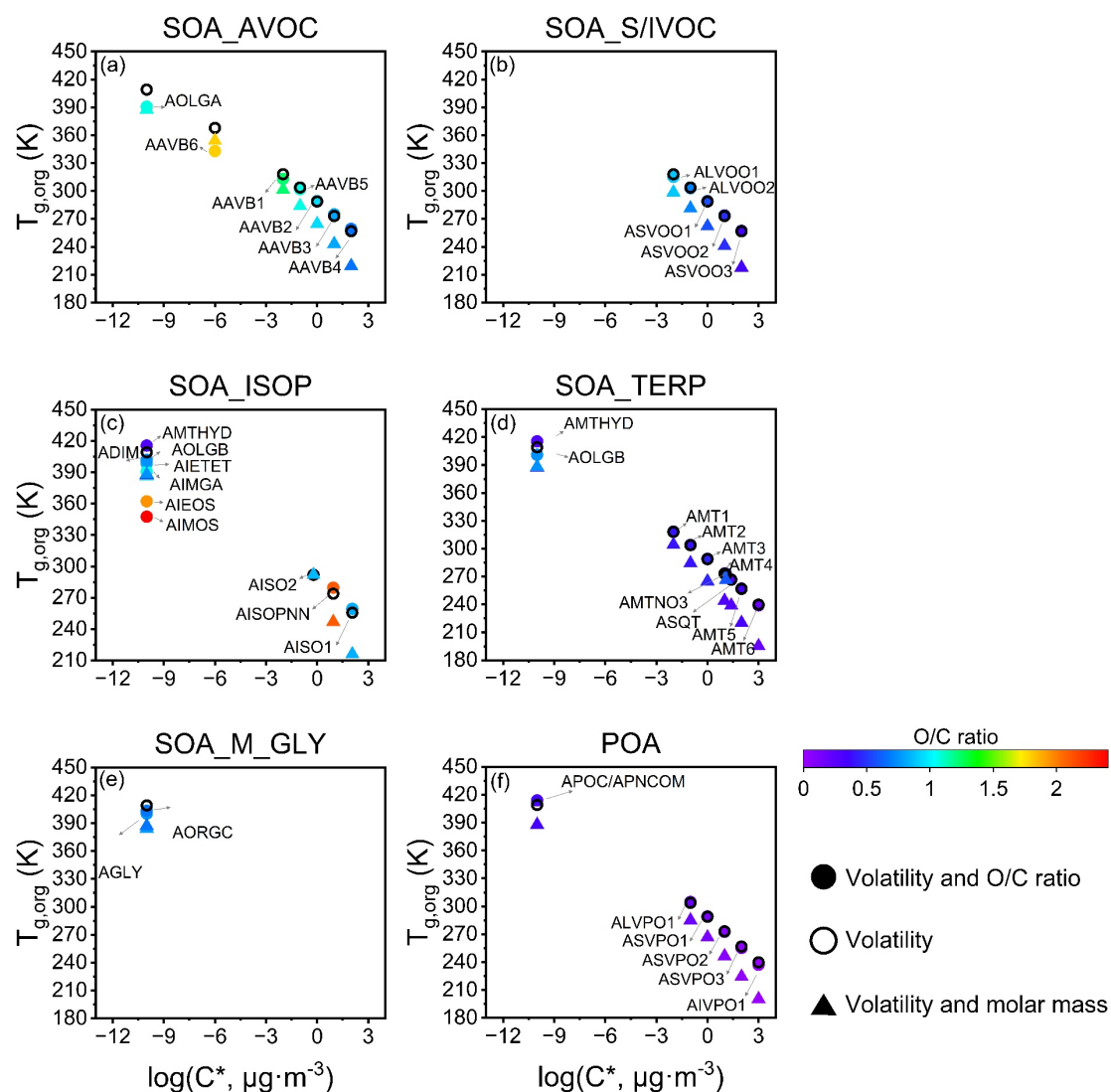


**Figure S18** Estimated  $T_{g,org}$  values for OA surrogate species. Solid circles represent  $T_{g,org}$  calculated using both volatility and O/C ratios, with colors indicating the O/C ratio, while open circles represent  $T_{g,org}$  calculated using volatility alone and solid triangles represent  $T_{g,org}$  calculated using volatility and molar mass (see Table S6 for a more detailed description of the CMAQ OA species).

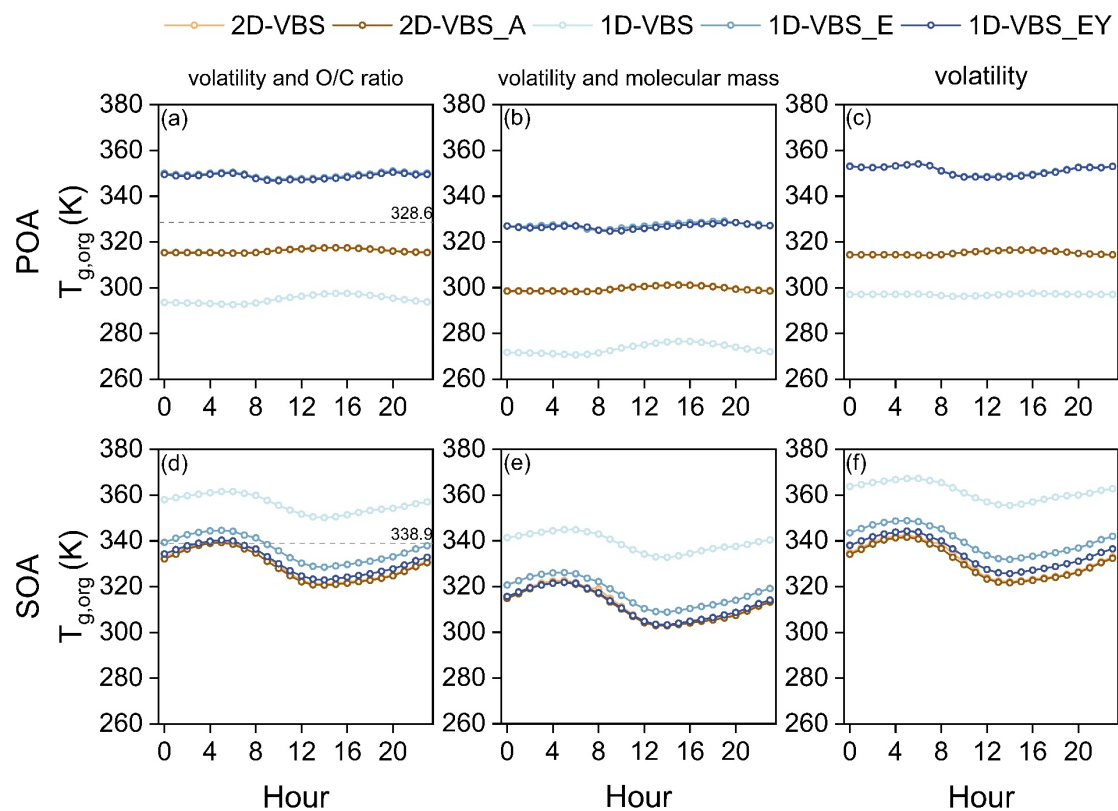


**Figure S19** Comparison of simulated diurnal variations of POA and SOA  $T_{g,org}$  with estimates based on observations in DY.  $T_{g,org}$  values were estimated using both volatility and O/C ratios (a)(d), volatility and molecular masses (b)(e), and volatility only (c)(f), respectively.

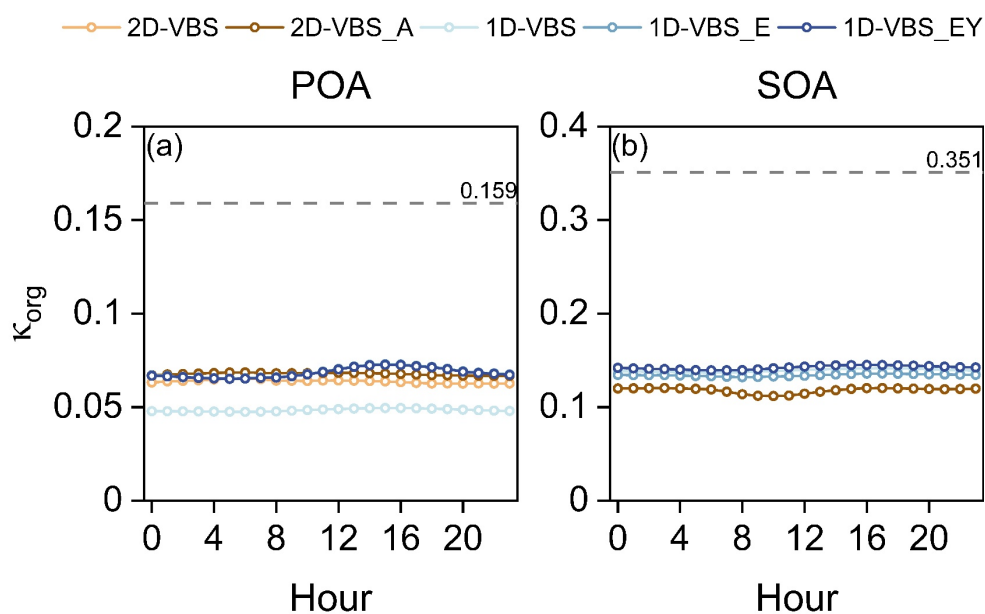


**Figure S20** Diurnal variation of (a) POA and (b) SOA  $\kappa_{\text{org}}$ , predicted as a function of OM/OC, with the grey dashed line representing the  $\kappa_{\text{org}}$  value derived from observations, estimated as a function of  $f_{44}$  (i.e., the fraction of  $m/z$  44 signal in total organic signals).



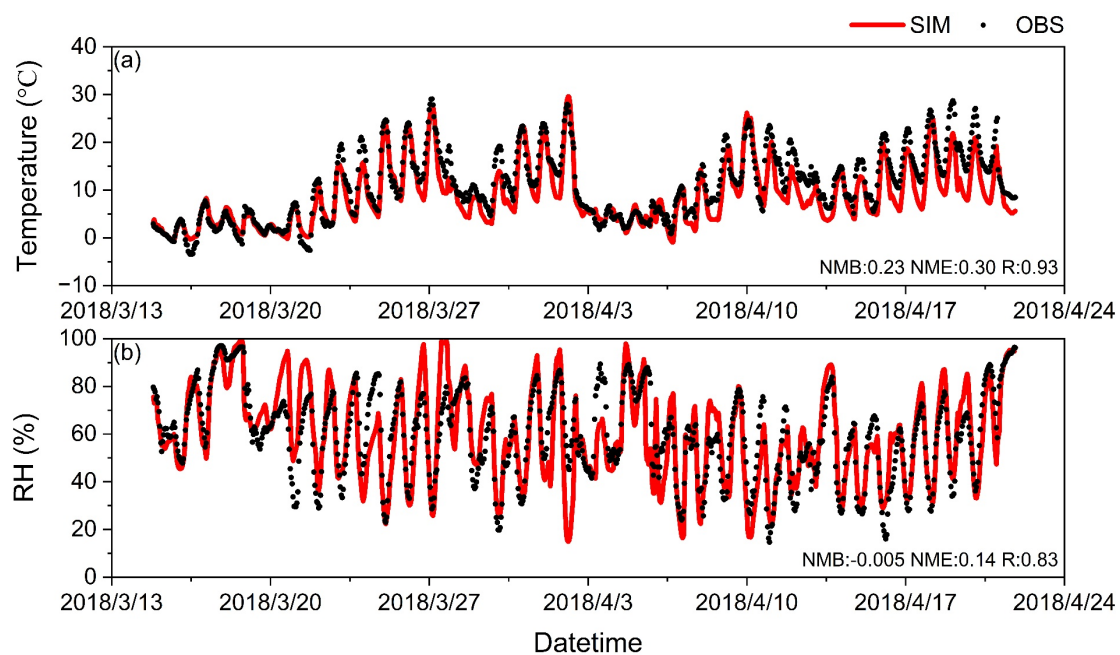


**Figure S21** Time series of (a) temperature (T) and (b) relative humidity (RH) at the DY site.

## Supplementary References

- An, J., Huang, C., Huang, D., Qin, M., Liu, H., Yan, R., Qiao, L., Zhou, M., Li, Y., Zhu, S., Wang, Q., and Wang, H.: Sources of organic aerosols in eastern China: a modeling study with high-resolution intermediate-volatility and semivolatile organic compound emissions, *Atmos. Chem. Phys.*, 23, 323-344, <https://doi.org/10.5194/acp-23-323-2023>, 2023.
- Bilsback, K. R., He, Y., Cappa, C. D., Chang, R. Y.-W., Croft, B., Martin, R. V., Ng, N. L., Seinfeld, J. H., Pierce, J. R., and Jathar, S. H.: Vapors Are Lost to Walls, Not to Particles on the Wall: Artifact-Corrected Parameters from Chamber Experiments and Implications for Global Secondary Organic Aerosol, *Environ Sci Technol*, 57, 53-63, <https://doi.org/10.1021/acs.est.2c03967>, 2023.
- Carlton, A. G., Turpin, B. J., Altieri, K. E., Seitzinger, S. P., Mathur, R., Roselle, S. J., and Weber, R. J.: CMAQ Model Performance Enhanced When In-Cloud Secondary Organic Aerosol is Included: Comparisons of Organic Carbon Predictions with Measurements, *Environ. Sci. Technol.*, 42, 8798-8802, <https://doi.org/10.1021/es801192n>, 2008.
- Carlton, A. G., Bhawe, P. V., Napelenok, S. L., Edney, E. O., Sarwar, G., Pinder, R. W., Pouliot, G. A., and Houyoux, M.: Model representation of secondary organic aerosol in CMAQv4.7, *Environ. Sci. Technol.*, 44, 8553-8560, <https://doi.org/10.1021/es100636q>, 2010.
- Chang, X., Zhao, B., Zheng, H., Wang, S., Cai, S., Guo, F., Gui, P., Huang, G., Wu, D., Han, L., Xing, J., Man, H., Hu, R., Liang, C., Xu, Q., Qiu, X., Ding, D., Liu, K., Han, R., Robinson, A. L., and Donahue, N. M.: Full-volatility emission framework corrects missing and underestimated secondary organic aerosol sources, *One Earth*, 5, 403-412, <https://doi.org/10.1016/j.oneear.2022.03.015>, 2022.
- Che, H., Shen, X., Yao, Z., Wu, B., Gou, R., Hao, X., Cao, X., Li, X., Zhang, H., Wang, S., and Chen, Z.: Real-world emission characteristics and inventory of volatile organic compounds originating from construction and agricultural machinery, *Sci. Total Environ.*, 894, 164993, <https://doi.org/10.1016/j.scitotenv.2023.164993>, 2023.
- Chen, Q., Miao, R., Geng, G., Shrivastava, M., Dao, X., Xu, B., Sun, J., Zhang, X., Liu, M., Tang, G., Tang, Q., Hu, H., Huang, R.-J., Wang, H., Zheng, Y., Qin, Y., Guo, S., Hu, M., and Zhu, T.: Widespread 2013-2020 decreases and reduction challenges of organic aerosol in China, *Nat. Commun.*, 15, 4465, <https://doi.org/10.1038/s41467-024-48902-0>, 2024.
- Chen, W., Ye, Y., Hu, W., Zhou, H., Pan, T., Wang, Y., Song, W., Song, Q., Ye, C., Wang, C., Wang, B., Huang, S., Yuan, B., Zhu, M., Lian, X., Zhang, G., Bi, X., Jiang, F., Liu, J., Canonaco, F., Prevot, A. S. H., Shao, M., and Wang, X.: Real - Time Characterization of Aerosol Compositions, Sources, and Aging Processes in Guangzhou During PRIDE - GBA 2018 Campaign, *J. Geophys. Res.*, 126, e2021JD035114, <https://doi.org/10.1029/2021JD035114>, 2021.
- Emery, C. and Tai, E.: Enhanced Meteorological Modeling and Performance Evaluation for Two Texas Ozone Episodes,
- Emery, C., Liu, Z., Russell, A. G., Odman, M. T., Yarwood, G., and Kumar, N.: Recommendations on statistics and benchmarks to assess photochemical model performance, *J. Air Waste Manag. Assoc.*, 67, 582-598, <https://doi.org/10.1080/10962247.2016.1265027>, 2017.
- Feng, T., Wang, Y., Hu, W., Zhu, M., Song, W., Chen, W., Sang, Y., Fang, Z., Deng, W., Fang, H., Yu, X., Wu, C., Yuan, B., Huang, S., Shao, M., Huang, X., He, L., Lee, Y. R., Huey, L. G., Canonaco, F., Prevot, A. S. H., and Wang, X.: Impact of aging on the sources, volatility, and viscosity of organic aerosols in Chinese outflows, *Atmos. Chem. Phys.*, 23, 611-636, <https://doi.org/10.5194/acp-23-611-2023>, 2023.
- Ge, X., Li, L., Chen, Y., Chen, H., Wu, D., Wang, J., Xie, X., Ge, S., Ye, Z., Xu, J., and Chen, M.: Aerosol

characteristics and sources in Yangzhou, China resolved by offline aerosol mass spectrometry and other techniques, *Environmental Pollution*, 225, 74-85, <https://doi.org/10.1016/j.envpol.2017.03.044>, 2017.

Gu, C., Cui, S., Ge, X., Wang, Z., Chen, M., Qian, Z., Liu, Z., Wang, X., and Zhang, Y.: Chemical composition, sources and optical properties of nitrated aromatic compounds in fine particulate matter during winter foggy days in Nanjing, China, *Environ.Res.*, 212, 113255, <https://doi.org/10.1016/j.envres.2022.113255>, 2022.

Huang, C., Hu, Q., Li, Y., Tian, J., Ma, Y., Zhao, Y., Feng, J., An, J., Qiao, L., Wang, H., Jing, S., Huang, D., Lou, S., Zhou, M., Zhu, S., Tao, S., and Li, L.: Intermediate Volatility Organic Compound Emissions from a Large Cargo Vessel Operated under Real-World Conditions, *Environ. Sci. Technol.*, 52, 12934-12942, <https://doi.org/10.1021/acs.est.8b04418>, 2018.

Kohl, I., Bachmann, L., Hallbrucker, A., Mayer, E., and Loerting, T.: Liquid-like relaxation in hyperquenched water at  $\leq 140$  K, *Physical Chemistry Chemical Physics*, 7, 3210-3220, 2005.

Li, K., Chen, L., White, S. J., Zheng, X., Lv, B., Lin, C., Bao, Z., Wu, X., Gao, X., Ying, F., Shen, J., Azzi, M., and Cen, K.: Chemical characteristics and sources of PM<sub>1</sub> during the 2016 summer in Hangzhou, *Environmental Pollution*, 232, 42-54, <https://doi.org/10.1016/j.envpol.2017.09.016>, 2018.

Lu, Q. Y., Murphy, B. N., Qin, M. M., Adams, P., Zhao, Y. L., Pye, H. O. T., Efstathiou, C., Allen, C., and Robinson, A. L.: Simulation of organic aerosol formation during the CalNex study: updated mobile emissions and secondary organic aerosol parameterization for intermediate-volatility organic compounds, *Atmos. Chem. Phys.*, 20, 4313-4332, <https://doi.org/10.5194/acp-20-4313-2020>, 2020.

McDonald, B., de Gouw, J., Gilman, J., Jathar, S., Akherati, A., Cappa, C., Jimenez, J., Lee-Taylor, J., Hayes, P., McKeen, S., Cui, Y., Kim, S.-W., Gentner, D., Isaacman-VanWertz, G., Goldstein, A., Harley, R., Frost, G., Roberts, J., Ryerson, T., and Trainer, M.: Volatile chemical products emerging as largest petrochemical source of urban organic emissions, *Science (New York, N.Y.)*, 359, 760-764, <https://doi.org/10.1126/science.aag0524>, 2018.

Murphy, B. N., Woody, M. C., Jimenez, J. L., Carlton, A. M. G., Hayes, P. L., Liu, S., Ng, N. L., Russell, L. M., Setyan, A., Xu, L., Young, J., Zaveri, R. A., Zhang, Q., and Pye, H. O. T.: Semivolatile POA and parameterized total combustion SOA in CMAQv5.2: impacts on source strength and partitioning, *Atmos. Chem. Phys.*, 17, 11107-11133, <https://doi.org/10.5194/acp-17-11107-2017>, 2017.

Pye, H. O. T., Luecken, D. J., Xu, L., Boyd, C. M., Ng, N. L., Baker, K. R., Ayres, B. R., Bash, J. O., Baumann, K., Carter, W. P. L., Edgerton, E., Fry, J. L., Hutzell, W. T., Schwede, D. B., and Shepson, P. B.: Modeling the Current and Future Roles of Particulate Organic Nitrates in the Southeastern United States, *Environ. Sci. Technol.*, 49, 14195-14203, <https://doi.org/10.1021/acs.est.5b03738>, 2015.

Pye, H. O. T., Pinder, R. W., Piletic, I. R., Xie, Y., Capps, S. L., Lin, Y.-H., Surratt, J. D., Zhang, Z., Gold, A., Luecken, D. J., Hutzell, W. T., Jaoui, M., Offenberg, J. H., Kleindienst, T. E., Lewandowski, M., and Edney, E. O.: Epoxide Pathways Improve Model Predictions of Isoprene Markers and Reveal Key Role of Acidity in Aerosol Formation, *Environ. Sci. Technol.*, 47, 11056-11064, <https://doi.org/10.1021/es402106h>, 2013.

Pye, H. O. T., Murphy, B. N., Xu, L., Ng, N. L., Carlton, A. G., Guo, H., Weber, R., Vasilakos, P., Appel, K. W., Budisulistiorini, S. H., Surratt, J. D., Nenes, A., Hu, W., Jimenez, J. L., Isaacman-VanWertz, G., Misztal, P. K., and Goldstein, A. H.: On the implications of aerosol liquid water and phase separation for organic aerosol mass, *Atmos. Chem. Phys.*, 17, 343-369, [10.5194/acp-17-343-2017](https://doi.org/10.5194/acp-17-343-2017), 2017.

Qin, M., Murphy, B. N., Isaacs, K. K., McDonald, B. C., Lu, Q., McKeen, S. A., Koval, L., Robinson, A. L., Efstathiou, C., Allen, C., and Pye, H. O. T.: Criteria pollutant impacts of volatile chemical products informed by near-field modelling, *Nature Sustainability*, 4, 129-137, 2021.

Shen, X., Che, H., Lv, T., Wu, B., Cao, X., Li, X., Zhang, H., Hao, X., Zhou, Q., and Yao, Z.: Real-world emission characteristics of semivolatile/intermediate-volatility organic compounds originating from nonroad construction machinery in the working process, *Sci. Total Environ.*, 858, 159970, <https://doi.org/10.1016/j.scitotenv.2022.159970>, 2023.

Simon, H. and Bhawe, P. V.: Simulating the Degree of Oxidation in Atmospheric Organic Particles, *Environmental Science & Technology*, 46, 331-339, 10.1021/es202361w, 2012.

Tang, R., Lu, Q., Guo, S., Wang, H., Song, K., Yu, Y., Tan, R., Liu, K., Shen, R., Chen, S., Zeng, L., Jorga, S. D., Zhang, Z., Zhang, W., Shuai, S., and Robinson, A. L.: Measurement report: Distinct emissions and volatility distribution of intermediate-volatility organic compounds from on-road Chinese gasoline vehicles: implication of high secondary organic aerosol formation potential, *Atmos. Chem. Phys.*, 21, 2569-2583, <https://doi.org/10.5194/acp-21-2569-2021>, 2021.

Xian, J., Cui, S., Chen, X., Wang, J., Xiong, Y., Gu, C., Wang, Y., Zhang, Y., Li, H., Wang, J., and Ge, X.: Online chemical characterization of atmospheric fine secondary aerosols and organic nitrates in summer Nanjing, China, *Atmos. Res.*, 290, 106783, <https://doi.org/10.1016/j.atmosres.2023.106783>, 2023.

Xu, J., Liu, D., Wu, X., Vu, T. V., Zhang, Y., Fu, P., Sun, Y., Xu, W., Zheng, B., Harrison, R. M., and Shi, Z.: Source apportionment of fine organic carbon at an urban site of Beijing using a chemical mass balance model, *Atmos. Chem. Phys.*, 21, 7321-7341, <https://doi.org/10.5194/acp-21-7321-2021>, 2021.

Xu, L., Pye, H. O. T., He, J., Chen, Y., Murphy, B. N., and Ng, N. L.: Experimental and model estimates of the contributions from biogenic monoterpenes and sesquiterpenes to secondary organic aerosol in the southeastern United States, *Atmos. Chem. Phys.*, 18, 12613-12637, <https://doi.org/10.5194/acp-18-12613-2018>, 2018.

Zhang, Y., Zhang, X., Zhong, J., Sun, J., Shen, X., Zhang, Z., Xu, W., Wang, Y., Liang, L., Liu, Y., Hu, X., He, M., Pang, Y., Zhao, H., Ren, S., and Shi, Z.: On the fossil and non-fossil fuel sources of carbonaceous aerosol with radiocarbon and AMS-PMF methods during winter hazy days in a rural area of North China plain, *Environ. Res.*, 208, 112672, <https://doi.org/10.1016/j.envres.2021.112672>, 2022.

Zhao, B., Wang, S., Donahue, N. M., Chuang, W., Hildebrandt Ruiz, L., Ng, N. L., Wang, Y., and Hao, J.: Evaluation of One-Dimensional and Two-Dimensional Volatility Basis Sets in Simulating the Aging of Secondary Organic Aerosol with Smog-Chamber Experiments, *Environ. Sci. Technol.*, 49, 2245-2254, <https://doi.org/10.1021/es5048914>, 2015.

Zhao, J., Qi, L., Lv, Z., Wang, X., Deng, F., Zhang, Z., Luo, Z., Bie, P., He, K., and Liu, H.: An updated comprehensive IVOC emission inventory for mobile sources in China, *Sci. Total Environ.*, 851, 158312, <https://doi.org/10.1016/j.scitotenv.2022.158312>, 2022.

Zheng, H., Chang, X., Wang, S., Li, S., Yin, D., Zhao, B., Huang, G., Huang, L., Jiang, Y., Dong, Z., He, Y., Huang, C., and Xing, J.: Trends of Full-Volatility Organic Emissions in China from 2005 to 2019 and Their Organic Aerosol Formation Potentials, *Environ. Sci. Technol. Lett.*, 10, 137-144, <https://doi.org/10.1021/acs.estlett.2c00944>, 2023.

Zhu, W., Zhou, M., Cheng, Z., Yan, N., Huang, C., Qiao, L., Wang, H., Liu, Y., Lou, S., and Guo, S.: Seasonal variation of aerosol compositions in Shanghai, China: Insights from particle aerosol mass spectrometer observations, *Sci. Total Environ.*, 771, 144948, <https://doi.org/10.1016/j.scitotenv.2021.144948>, 2021.